Stabilization of Black Phosphorus using Sonication-Assisted Simultaneous Exfoliation-Functionalization

Maart van Druenen[a,b], Timothy Collins[a,b], Fionán Davitt[a,b], Jessica Doherty[a,b], Gillian Collins[a,b], Zdeněk Sofer[c,*] and Justin D. Holmes[a,b,*]

Abstract: Black Phosphorus (BP) displays extraordinary properties but its ambient instability remains a critical challenge. Functionalization has been employed to overcome the sensitivity of BP to ambient conditions while preserving its properties. Here, we report a simultaneous exfoliation-functionalization process that functionalizes BP flakes during exfoliation, hence providing increased protection which can be attributed to the minimal exposure of flakes to ambient oxygen and water. A tetrabutylammonium salt was employed for the intercalation of BP, resulting in the formation of flakes with large lateral dimensions. The addition of an aryl iodide or an aryl iodonium salt to the exfoliation solvent creates a scalable strategy for the production of functionalized few-layer BP flakes. The ambient stability of functionalized BP was prolonged to a period of 1 week compared to unfunctionalized BP, as characterized using scanning transmission electron microscopy (STEM), atomic force microscopy (AFM) and x-ray photoelectron spectroscopy (XPS).

Introduction

The last few years have seen an immense interest in 2D materials which show promise in a number of applications.[1] In particular, BP is a promising new 2D material which displays exceptional properties.[2] The high carrier mobility and layer tunable bandgap range (0.3 - 2 eV) that falls in between graphene and transition metal dichalcogenides make it ideal for a range of applications including electrical,[3] energy storage[4] and optical devices.[5] While BP shows extraordinary properties, its application is hindered by its degradation under ambient conditions.[6] The lifetime of BP has been extended using covalent functionalization,[7] non-covalent functionalization,[8] solvents,[9] polymers[10] and fluorination[11] which protect BP from reaction with ambient water and oxygen, and can also enhance its properties for various applications. While the study of the surface chemistry and covalent modification is crucial for future application of the material, it remains largely undiscovered.

[a] Dr. Maart van Druenen, Dr. Timothy Collins, Dr. Fionán Davitt, Dr. Jessica Doherty, Dr. Gillian Collins, prof. Justin D. Holmes
School of Chemistry, Environmental Research Institute & Tyndall National Institute, University College Cork, Cork, T12 YN60, Ireland.
Tel: +353 (0)21 4903608;
E-mail: j.holmes@ucc.ie
Central Laboratories, University of Chemistry and Technology Prague, Technická 5, 166 28 Prague 6, Czech Republic
[b] Dr. Maart van Druenen, Dr. Timothy Collins, Dr. Fionán Davitt, Dr. Jessica Doherty, Dr. Gillian Collins, prof. Justin D. Holmes
AMBER@CRANN, Trinity College Dublin, Dublin 2, Ireland
[c] Prof. Dr. Zdenek Sofer
Department of Inorganic Chemistry, University of Chemistry and Technology Prague, Technická 5, 166 28 Prague 6, Czech Republic.
E-mail: zdenek.sofer@vscht.cz

Covalent functionalization has been achieved using nucleophilic reagents,[7b] azide modification,[12] iodonium salts[7c] and diazonium salts[7a] which enhanced the stability up to 25 days. Functionalization using diazonium salts has also been achieved by a single step exfoliation-functionalization process using wet-jet milling.[7k] Wild et. al.[7d] used K and Na intercalation compounds to exfoliate and reduce the BP surface for subsequent reaction with alkyl halides. Intercalation compounds have been widely used for the exfoliation and reduction of graphene,[13] however, their use with BP remains limited.[14] Alkali metals have been used to alter the properties of BP[15] but the resulting intercalation complexes suffer from poor ambient stability[16] while intercalation using alkylammonium salts can stabilize BP.[17] Tetrabutylammonium salts have been used for the formation of BP intercalation compounds under electrochemical conditions which enhanced the efficiency of exfoliation,[18] while ammonium salts have proven to have a facilitative effect on BP exfoliation through edge intercalation which overcomes the interlayer van der Waals forces.[14b] Here, a scalable protection strategy is presented where simultaneous exfoliation and functionalization is achieved through sonication of BP in a tetrabutylammonium and aryl iodide solution. The addition of the tetrabutylammonium salt facilitates exfoliation by acting as an intercalation agent, in correlation with theoretical studies.[17] Tetrabutylammonium salts have been used as intercalation agents to form graphene[19] and black phosphorus[16-17] intercalation complexes and have also been reported to promote the exfoliation of 2D materials.[18]

Recently, in-situ radical polymerization with poly(methyl methacrylate) (PMMA) under sonication has been employed to form a BP-polymer hybrid.[10a] Ultrasonication has been employed for the fluorination of BP[11c] and simultaneous exfoliation and covalent modification of graphene[20] while it has also been shown to improve the efficiency of carbon nanotube functionalization.[21] The addition of the functionalization reagent during the exfoliation process ensures functionalization directly after exfoliation, which significantly enhances the ambient stability due to the minimal exposure to ambient oxidants, such as oxygen and water. BP oxidation has been proposed to occur at defect sites,[22] with the formation of an initial surface oxide catalyzing further oxidation, and therefore a functionalization strategy that protects oxygen defects during the exfoliation procedure when few-layer flakes are produced is highly desirable. Furthermore, the one-step process using aryl iodides enables the scalable production of functionalized few-layer BP flakes. Aryl iodides have been employed for the functionalization of carbon surfaces,[23] carbon nanotubes[24] and graphene[25] while offering a number of advantages over diazonium and iodonium salts, including commercial availability and lower reactivity which allows greater control over the functionalization layer thickness.[23]

Here, we present the simultaneous exfoliation and functionalization of BP using a sonochemical approach. The production of high-quality exfoliated phosphorene nanosheets is demonstrated using STEM, TEM, AFM and Raman analysis, while

the functionalized flakes are also analysed using XPS and attenuated total reflectance Fourier transform infrared (ATR-FTIR) spectroscopy to confirm successful covalent modification and to characterize the surface chemistry. The addition of tetrabutylammonium facilitates exfoliation and results in the formation of flakes with large lateral dimensions. STEM, AFM and XPS analysis confirm the ambient stability was successfully prolonged to a period of 1 week.

Results and Discussion

BP was synthesized using vapor-phase growth[26] and characterized using XPS and Raman analysis, as displayed in Figure S1 (see Supporting Information). The P 2p core level displays a 15.3 % oxide shoulder at 132.1 eV compared to the main P 2p peak. The Raman modes at 367, 444 and 473 cm^{-1} correspond to the A^1_g, B^2_g and A^2_g vibrational modes.[9a] The Raman modes and low amount of oxidation observed in the P 2p core level indicate a high crystal quality with a minimal amount of oxide after synthesis. Exfoliation and functionalization was carried out by sonication of the BP crystals in a 4-iodobenzenetrifluoride (IBF) and tetrabutylammonium hexafluorophosphate (TBAFP) solution in NMP. Figure 1 displays the production of few-layer BP flakes which were characterized using STEM, TEM and AFM to evaluate the effect of exfoliation and functionalization on crystallinity. STEM analysis displays the formation of few-layer BP flakes, as shown in Figures 1(a) and S2(a)-(c). TEM analysis, as shown in Figure S2(d), depicts the crystal lattice with d-spacings of 1.83 and 2.66 Å. The selected area electron diffraction (SAED) pattern in Figure 1(c) also displays d-spacings of 1.53, 1.86, 2.65 and 3.47 Å, corresponding to the (200), (121), (111) and (010) planes of BP.21,50,51 Raman characterization displays the A^1_g, A^2_g and B^2_g peaks at 366, 444, 473 cm^{-1}, in correlation with literature reports.[9a, 27] TEM and Raman analysis indicate that the BP flakes maintain their crystallinity during the exfoliation-functionalization process. AFM analysis in Figures 1(e) and (f) shows a height of ~27 nm for IBF functionalized BP and ~16 nm for FPI functionalized BP, confirming the production of few-layer flakes. Further AFM analysis, shown in Figure S3, highlights the production of flakes with heights in the 10-26 nm range. The role of TBAFP was investigated by comparing the heights and lateral dimensions of exfoliated flakes. Figure S4 displays the heights of BP exfoliated using (1) standard exfoliation in NMP under sonication, (2) exfoliation under sonication in an IBF solution without the presence of an intercalating agent (TBAFP), (3) exfoliation under sonication in the presence of IBF and an intercalating agent (TBAFP) and (4) step-wise exfoliation by exposure to a solution of the intercalating agent, followed by minimal sonication (10 min) and then the addition of IBF. Table S1 shows an increase in few-layer flakes for BP exfoliated in a solution of IBF and TBAFP under continuous sonication. The percentage of flakes with heights <10 nm was 54 % for BP exfoliated in IBF with the presence of the intercalating agent (TBAFP) and a similar percentage (50 %) was obtained for those exfoliated in FPI and TBAFP. The standard BP exfoliated under sonication (without IBF and TBAFP) only showed 11 % of flakes with heights < 10 nm which was comparable to BP exfoliated without the presence of the intercalating agent and in the stepwise exfoliation with minimal sonication, which both resulted in 19 % of flakes with heights < 10 nm. The increase in few-layer flakes for BP exfoliated in the presence of TBAFP suggests it has a facilitative effect on exfoliation. Figure S5 and Table S2 show the lateral dimensions of the corresponding samples, indicating that the addition of TBAFP facilitates the formation of BP flakes with large lateral dimensions. BP exfoliated in the presence of IBF and TBAFP produced 59 % flakes with a length >0.5 µm and 30 % with lengths >1 µm, compared to BP which only provides 9 % flakes with lengths >0.5 µm and did not result in the production of flakes with dimensions greater than 1 µm. The exfoliation of BP in the presence of IBF and TBAFP but without constant sonication also showed a slight increase in the production of few-layer flakes with large lateral dimensions compared to BP, but continuous sonication greatly increased the formation of few-layer flakes with larger lengths. The intercalation of 2D materials is aided by sonication which allows faster diffusion of intercalating species.[14b] The increased amount of few-layer flakes with large lateral dimensions for BP exfoliated in the presence of TBAFP under minimal sonication indicates it acts as an intercalating agent that facilitates exfoliation, in correlation with theoretical studies,[17] although prolonged sonication promotes the separation of the layers and aids intercalation.[14b] TBA salts have been used for graphene intercalation due to the flexibility of the n-butyl chains[19a, d] while the butyl chain length is optimal for BP intercalation compared to tetramethyl and tetraoctylammonium cations.[18b] The flattened configuration of TBA displays a diameter of 0.47 nm which closely matches the 0.53 nm interlayer spacing of BP, also allowing efficient intercalation[18b, 28] The intercalation enhances the formation of few-layer flakes with large lateral dimensions which is beneficial for device applications.

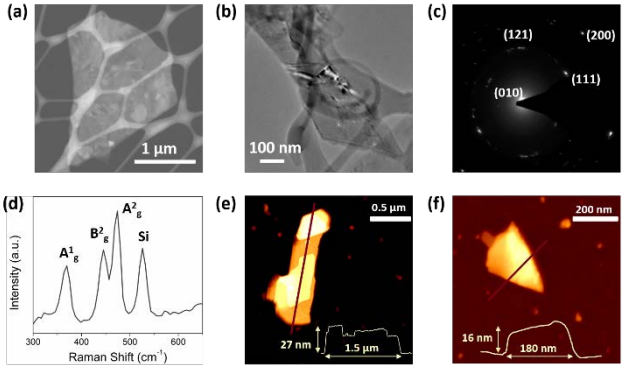

Figure 1. (a) STEM, (b) TEM analysis, (c) a SAED pattern and (d) Raman analysis display the crystallinity of IBF-functionalized BP. AFM analysis of (e) IBF and (f) FPI functionalized BP confirms the formation of few-layer flakes.

The characterization of functionalized BP flakes using ATR-FTIR analysis indicates reaction of aryl groups with BP. Figure 2 displays the ATR-FTIR analysis of IBF-functionalized BP which shows the presence of a para-substituted out-of-plane C-H bend at 845 cm^{-1}, an in-plane C-H bend at 1014 cm^{-1}, asymmetric CF_3

stretches at 1149 and 1120 cm^{-1} and a symmetric CF_3 stretch at 1318 cm^{-1}, confirming covalent functionalization of the aryl group.[29] The PF_6^- anion cannot be observed at 825 and 737 cm^{-1}, indicating the absence of the counterion on BP.[30] The ATR-FTIR analysis of FPI-functionalized BP is displayed in Figure S6. Similarly, covalent attachment can be observed through the presence of out-of-plane C-H stretches at 800 and 845 cm^{-1}, an in-plane C-H stretch at 1028 cm^{-1} and a C-F stretch at 1260 cm^{-1}.[31] Additionally, the minor presence of a symmetric S=O stretch at 1152 cm^{-1} suggests passivation of the triflate counterion.[30a]

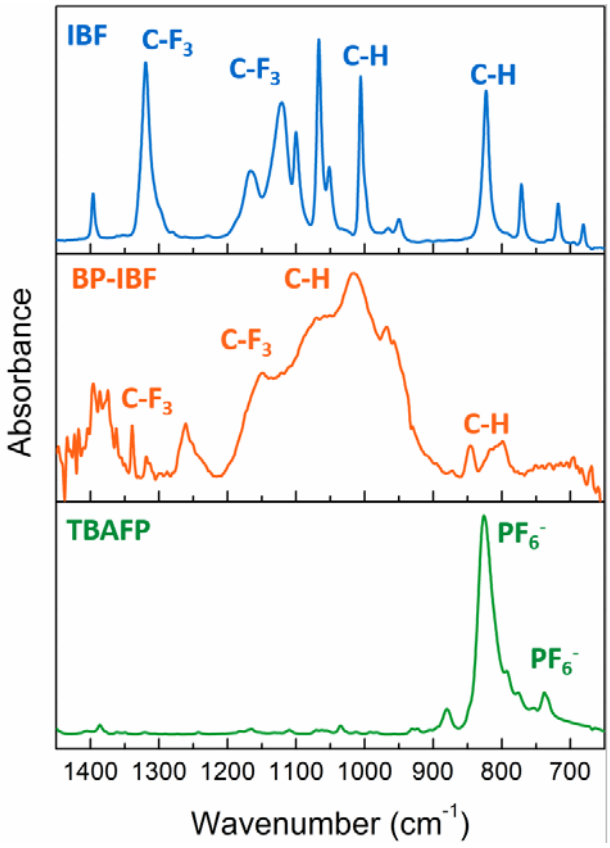

Figure 2. ATR-FTIR analysis of IBF, IBF modified BP and TBAFP.

XPS analysis was used to further characterize the surface chemistry of aryl-functionalized BP. Functionalization of BP using FPI (20.1 %) and IBF (20.8 %) resulted in minimal oxidation after exfoliation and functionalization, based on analysis of the P 2p core level, as displayed in Figures 3 and S5. Figure 3(a) shows the absence of the I 3d peak at ~619 eV indicating dissociation of the aryl iodide and subsequent arylation of BP. The F 1s peak shows a contribution at 687 eV which can be attributed to the CF_3 group, suggesting the presence of the CF_3 substituted aryl group on the surface. The F 1s peak also displays a contribution at 691.6 eV, which can be attributed to the fluorination of BP.[11a, b] As the electrolyte also contains a source of fluorine, functionalization using only TBAFP was carried out to confirm the F 1s signal can be attributed to the CF_3 group rather than the PF_6^- counterion. Figure S7 displays XPS analysis of BP exfoliated in a solution of TBAFP. The absence of a F 1s signal at 687 eV indicates the F 1s peak observed for the IBF functionalized sample can be attributed to the CF_3 aryl group rather than the PF_6^- counterion. Furthermore, the absence of a contribution in the P 2p core level at 136.5 eV confirms the absence of PF_6^- in IBF-functionalized BP. Functionalization using FPI was also characterized using XPS analysis as shown in Figure S8 which shows the absence of an I 3d peak and the presence of a F 1s peak at 688.5 eV, indicative of the attachment of the fluorinated aryl group. In combination, ATR-FTIR and XPS of the F 1s core level confirm the covalent attachment of aryl groups on BP using an aryl iodide (IBF) and a diaryliodonium salt (FPI).

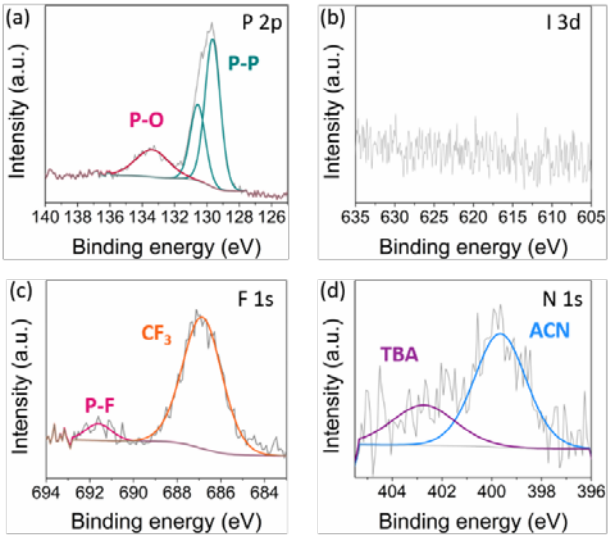

Figure 3. XPS analysis displaying the (a) P 2p, (b) I 3d, (c) F 1s and (d) N 1s core levels of IBF functionalized BP).

The N 1s core level gives further insight into the surface passivation and more specifically the role of the electrolyte, tetrabutylammonium hexafluorophosphate (TBAFP). When the functionalization process was carried out without the presence of TBAFP a F 1s signal was not observed, suggesting functionalization did not occur (Figure S9). The need for TBAFP during functionalization is in agreement with literature reports; the covalent functionalization of BP using iodonium and diazonium salts only gives a high extent of functionalization in the presence of TBAFP.[7a-c, 19e] The extent of TBAFP passivation was quantified using the XPS analysis. The N 1s peak for IBF-functionalized BP shows a peak at 400.0 eV attributed to solvent passivation and at 402.7 eV corresponding to the binding energy (BE) of tetrabutylammonium (TBA), as displayed in Figure 3(d). When BP is exfoliated in a solution of TBAFP alone (Figure S7) the absence of a F 1s peak indicates the PF_6^- counterion of TBAFP does not bind to the surface. Additionally, the P 2p peak does not display a contribution for PF_6^- which is observed at 136.5 eV. The absence of a discernible contribution in the P 2p peak associated with PF_6^- indicates TBAFP does not passivate the surface, but rather the TBA interacts with the surface. TBA salts have been reported to facilitate exfoliation[32] and have also been employed as intercalation agents.[19a-d] Therefore TBA may play a similar role in the exfoliation of BP which was evaluated by carrying out a stepwise exfoliation-functionalization procedure, by immersion in a TBAFP solution, followed by minimal sonication (10 min) to separate BP layers and subsequent functionalization using IBF. The role of TBA as an intercalating agent is confirmed by the AFM analysis where few-layer flakes (2.5 - 15 nm) are produced when exfoliation is carried out in the presence of TBA with minimal sonication, as displayed in Figure S10. Exfoliation in the presence

of TBAFP resulted in 19 % of flakes with heights greater than 10 nm, an increase compared to the exfoliation of BP without the presence of TBAFP (11 %), considering the solution was subjected to minimal sonication. TBAFP has been employed as an intercalating agent for the exfoliation of graphene and black phosphorus[16-18] while it has been reported to facilitate exfoliation of layered oxides, hydroxides[33] and perovskites,[34] in correlation with our results. The addition of an IBF solution after intercalation and sonication also resulted in the covalent attachment of aryl groups. The presence of a F 1s peak (Figure S11) indicates the covalent attachment of the aryl group. TBAFP is often added as an electrolyte during the functionalization of 2D materials using aryldiazonium salts[7a, 35] but its role is rarely defined, although the addition has been reported to increase the degree of functionalization.[36] Enhanced functionalization has been attributed to the intercalation of flakes and stabilization after exfoliation which allows increased accessibility of the functionalization reagent to the basal plane.[19e, 37] The exact role of TBAFP remains unclear but the low extent of functionalization in the absence of TBAFP suggests it plays a critical role during functionalization.

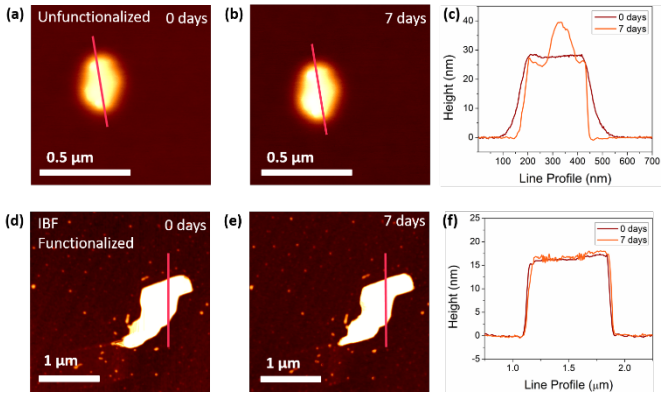

Figure 4. AFM analysis of IBF-functionalized BP during (a) 0 to (b) 7 days of ambient exposure and unfunctionalized BP during (d) 0 to (d) 7 days of ambient exposure. Corresponding line profiles for (c) IBF-functionalized and (f) unfunctionalized BP show the surface topography.

The binding of aryl groups to BP has been reported to occur through P-sites, either through cleavage of a P-P bond or insertion of a P-C bond resulting in the formation of a four-coordinate P which can create lattice distortion.[7a] DFT studies have suggested the cleavage of a P-P bond takes place when covalent attachment occurs which results in the formation of a 3-coordinate phosphorus with 2 P-P bonds and 1 P-C bond.[7b, d] The characterization of P-C bonds is difficult due to their low concentration and proximity in BE to P-O bonds in the P 2p core level. The attachment of aryl groups could also occur through attachment to existing surface oxide sites which has been observed previously.[7b, c, 38] The inhibition of the oxide formation over a period of 1 week also confirms this reaction mechanism (Figure S13), as binding to surface oxide sites prevents further oxidation of the BP.[7c]

Liquid exfoliation often results in solvent passivation which is undesirable for the processing of flakes, as the remaining solvent can have an adverse effect on the electrical characteristics of BP.[39] While a contribution is seen at ~400 eV, the combined exfoliation-functionalization process significantly reduces solvent passivation. Figure S12 displays the N 1s:P 2p ratios which can be used as an indication of the extent of solvent passivation. Unfunctionalized BP displays a N 1s:P 2p ratio of 0.49 while IBF-functionalized BP results in a reduction to 0.2, indicating the covalent attachment results in disruption of the solvent passivation layer. The N 1s:P 2p ratio reduces over a period of 1 week for both bare and IBF-functionalized BP. The decrease of 60 % in the N 1s:P 2p ratios for FPI and IBF-functionalization compared to unfunctionalized BP indicates functionalization successfully removes a large amount of solvent passivation making BP more suitable for device fabrication.

The passivation of BP with aryl groups results in a significant increase in the ambient stability of BP. AFM analysis was used to monitor the oxidation of a functionalized and an unfunctionalized flake over a 1 week period. Figure 4(a) shows an unfunctionalized flake with a height of ~27 nm, which displays defined edges and a flat surface. Ambient exposure of the flake for 1 week resulted in the formation of a large bump on the flake surface and degradation of the flake edges, which can be attributed to oxidation, as shown in Figures 4(b)-(c). In comparison, the functionalized BP flake has a height of ~16 nm, which did not show signs of deterioration during 1 week of ambient exposure and maintains its flat surface, as displayed in Figures 4(d)-(f).

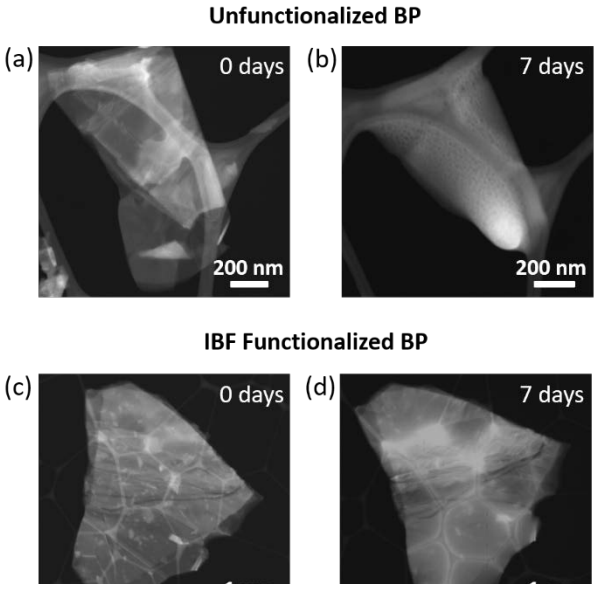

Figure 5. TEM analysis of unfunctionalized BP at (a) 0 days and (b) 7 days. IBF-functionalized BP at (c) 0 days and (d) 7 days.

The increased ambient lifetime of functionalized BP was also confirmed using STEM analysis, as shown in Figure 5. While 1 week of ambient exposure results in the disintegration of the BP flake, IBF-functionalization allows preservation of the flake morphology. The loss of edges for unfunctionalized BP can be seen in Figures 5(a)-(b) and the surface becomes covered in protrusions due to the formation of liquid phosphorus oxidation products.[6a] The IBF-functionalized BP flake surpasses the ambient stability of unfunctionalized BP, as shown in Figures 5(c)-(d). The flake edges remained defined during a 1 week period, while Figure 5(b) displays the absence of surface protrusions demonstrating the high stability of IBF-functionalized BP.

XPS analysis gives a spectroscopic representation of the superior ambient stability of functionalized BP by evaluation of the P 2p and O 1s core levels. The P 2p core level can be used to monitor BP oxidation, as the oxide shoulder at 132-136 eV can be

attributed to the formation of P-O species. Figures S13(a)-(b) display the evolution of the P 2p and O 1s core levels of unfunctionalized BP, FPI and IBF functionalized BP. The P 2p core level of freshly exfoliated BP displays an oxide shoulder of 32.7 % compared to the main P 2p peak, which increases to 36.7 % after 2 days and 63.6 % after 1 week. In comparison, the IBF-functionalized BP shows an oxide component of 20.8 % with 2 days of ambient exposure resulting in an increase to 24.2 % and a further increase to 38.0 % after a week period. Similarly, FPI displays a 20.1 % oxide component which rises to 26.9 % and 32.6 % after a 2 day and 1 week period, respectively. The minor increase in the oxide component of the P 2p core level of IBF and FPI-functionalized BP compared to unfunctionalized BP confirms its low reactivity in ambient conditions.

BP oxidation occurs through the formation of bridged and non-bridged oxide species.[6a, b, 40] While the P 2p component gives an indication of the total oxidation, the O 1s peak allows deconvolution of the bridging and non-bridging species giving further insight into BP oxidation. The evolution of the P-O-P component can be used as an indication of the extent of oxidation, as P-O-P species react further to form volatile phosphoric acids which are not detected using XPS analysis due to their volatility under vacuum.[6a, 22, 41] Exfoliation of bare BP displays a 12.3 % P-O-P component compared to the total O 1s component. The P-O-P component further increases to 20.3 % after 2 days and 43.3 % after a period of 1 week in ambient conditions, as shown in Figure S13. IBF-functionalization results in the formation of a similar amount of bridged oxide species (14.5 %) which decreases to 4.8 % after 2 days and 5.2 % after 1 week. FPI did not form a significant amount of P-O-P species (1.8 %). Similarly only a minor amount of P-O-P species were detected over a period of 1 week (3.6 %). Exfoliation of functionalized and unfunctionalized BP results in a similar amount of P-O-P formation, however, after initial oxide formation unfunctionalized BP appears to oxidize further at a considerable rate. The decrease in the P-O-P component for IBF-functionalized BP can be attributed to the evaporation of the volatile phosphorus oxides in the high vacuum XPS chamber.[7c] Additional oxidation of functionalized BP is inhibited and followed by removal of phosphorus oxides. FPI functionalization resulted in minimal P-O-P generation and subsequently only displays minor oxidation over a 1 week period. The P 2p and O 1s core levels indicate IBF and FPI-functionalized BP display superior ambient stability compared to unfunctionalized BP. Oxidation of BP occurs through reaction of oxygen with the BP surface forming non-bridging oxide species which convert to non-bridging species and then phosphoric oxyacids.[6a] Therefore a functionalization strategy that inhibits the formation of P-O-P species preserves the BP and significantly protects it from further oxidation.

Conclusions

The simultaneous exfoliation and functionalization of BP was used to produce few-layer flakes with enhanced ambient stability. AFM analysis was used to demonstrate the role of TBA as an intercalating agent that resulted in the formation of a higher proportion of few-layer flakes with large lateral dimensions. The surface chemistry of IBF-functionalized BP was characterized using XPS and ATR-FTIR, which revealed aryl functionalization. Aryl functionalization likely occurred through attachment to P- and O-sites, giving enhanced stability of up to 1 week, as demonstrated using STEM, AFM and XPS analysis. The simultaneous exfoliation and functionalization ensures immediate functionalization which greatly minimizes the oxidation of BP, while solvent passivation is minimized by functionalization. The reduction in solvent passivation and formation of few-layer flakes with large lateral dimensions demonstrates the simultaneous exfoliation-functionalization produces flakes more suitable for device fabrication.

Experimental Section

BP was synthesized using vapor-phase growth using a previously published procedure.[26] Red phosphorus (99.999%, Sigma-Aldrich, Czech Republic) was placed in quartz glass ampoule (25 mm inner diameter × 120mm length) together with 120 mg of Sn and 60 mg of SnI_4 and melt sealed under high vacuum (1×10^{-3} Pa). The ampoule was placed horizontally in a muffle furnace and heated to 650 °C over a period of 8 h and after 5 h the temperature was cooled to 400 °C for 50 h and finally to room temperature over a period of 25 h. The ampoule was opened in an Ar filled glovebox and repeatedly washed in DMF/carbon disulfide mixture and with pure carbon disulfide and finally dried under vacuum for 24 h. SnI_4 was made by direct reaction of Sn (99.999 %, Sigma-Aldrich, Czech Republic) and Iodine (99.999 %, Sigma-Aldrich, Czech Republic) in chloroform. The crystals obtained were recrystallized from chloroform.

Anhydrous N-methyl-2-pyrrolidone (NMP), acetonitrile (ACN), dimethylformamide (DMF) were purchased from Sigma-Aldrich. Solvents were subjected to 2 purification cycles to remove traces of oxygen and water. One cycle consists of drying over molecular sieves for at least 24 h, degassing using at least 10 freeze-pump-thaw cycles and purging the solvent with Ar for at least 30 min. BP was synthesized using vapor-phase growth as described previously. All solvent transfer and handling of BP prior to exfoliation was carried out in a glovebox. BP was exfoliated in (1) a solution of NMP, (2) a 50 mM solution of 4-iodobenzotrifluoride (IBF) with 20 mM tetrabutylammonium hexafluorophosphate (TBAFP), (3) a 50 mM solution of bis(4-fluorophenyl)iodonium triflate (FPI) with 20 mM TBAFP for 10 h in a Schlenk flask under constant flow of Ar using a bath sonicator (Branson 1800). The intercalated sample was immersed in a TBAFP solution for 24 h followed by sonication for 10 min and the addition of an IBF solution for 12 h. The functionalized BP solution was centrifuged at 2000 rpm for 30 min to exclude unexfoliated material and the supernatant was centrifuged at 14500 rpm for 30 min to obtain an exfoliated sample. The sample was purified using three acetonitrile washes and drop cast onto a Si or titanium coated Si wafer for further analysis.

X-ray photoelectron spectroscopy (XPS) was completed on an Oxford Applied Research Escabase XPS system (base pressure 5 × 10-10 mbar) and a nonmonochromated Al kα X-Ray source at 200 W. Survey spectra were collected at a pass energy of 100 eV, a step size of 0.7 eV, a dwell time of 0.3 s in the 0-1000 eV range. Core level spectra were recorded at a pass energy of 20 eV, a step size of 0.1 eV and a dwell time of 0.1 s. CasaXPS software was used to process spectra with peaks corrected to a Shirley background and fitted to Voigt profiles. Charge correction was applied using the C 1s peak at 285 eV. Attenuated total reflectance Fourier transform infrared (ATR-FTIR) were collected using a Nicolet 6700 Infrared Spectrometer with a liquid cooled MCT detector and a Smart iTR accessory. Spectra were collected in ambient conditions at a resolution of 2 cm^{-1} and averaged over 100 scans. UV analysis was completed on a Thermo Scientific Evolution 60 S UV-Visible spectrophotometer with a resolution of ±0.8 nm using a Xenon light source.

Raman scattering spectra were acquired using a QE65PRO OceanOptics spectrometer with a 50 µm width slit and a microscope with a 40 × objective to focus on the surface of substrates. A Laser Quantum GEM DPSS 532 nm laser was used for excitation. Transmission electron microscopy (TEM) analysis was performed on an FEI Titan electron microscope operating at 300 kV. Scanning transmission electron microscopy (STEM) was carried out on an FEI Helios Nanolab 600i scanning electron microscope operating at 20 kV. AFM analysis was carried out on a Park XE-100 AFM in non-contact mode with SSS_NCHR enhanced resolution tips with XY and Z resolutions of ~2 and 0.05 nm respectively.

Acknowledgements

This research was funded by the Irish Research Council Government of Ireland Postgraduate Scholarship Programme under grant number GOIPG/2015/2933 and Science Foundation Ireland under grant number 12/RC/2278. Z.S. was supported by Czech Science Foundation (GACR No. 19-26910X.

Keywords: Phosphorene • Black Phosphorus • Surface Functionalization • Surface Protection

[1] a) D. Geng and H. Y. Yang, *Adv Mater* **2018**, *30*, 1800865; b) F. Wang, Z. Wang, C. Jiang, L. Yin, R. Cheng, X. Zhan, K. Xu, F. Wang, Y. Zhang and J. He, *Small* **2017**, *13*, 1604298; c) S. Zhang, S. Guo, Z. Chen, Y. Wang, H. Gao, J. Gomez-Herrero, P. Ares, F. Zamora, Z. Zhu and H. Zeng, *Chem Soc Rev* **2018**, *47*, 982-1021; d) L. Li, P. Boullay, J. Cheng, P. Lu, X. Wang, G. Steciuk, J. Huang, J. Jian, X. Gao, B. Zhang, S. Misra, X. Zhang, K. Yang and H. Wang, *Materials Today Nano* **2019**, *6*, 100037; e) W. Ying, A. Khan and X. Peng, *Materials Today Nano* **2020**, *10*, 100074; f) N. R. Glavin, R. Rao, V. Varshney, E. Bianco, A. Apte, A. Roy, E. Ringe and P. M. Ajayan, *Advanced Materials* **2019**, *32*, 1904302.
[2] a) P. Chen, N. Li, X. Chen, W.-J. Ong and X. Zhao, *2D Materials* **2017**, *5*, 014002; b) R. Gusmao, Z. Sofer and M. Pumera, *Angew. Chem. Int. Ed.* **2017**; c) J. Sturala, Z. Sofer and M. Pumera, *Angew Chem Int Ed Engl* **2019**, *58*, 7551-7557.
[3] a) L. Li, Y. Yu, G. J. Ye, Q. Ge, X. Ou, H. Wu, D. Feng, X. H. Chen and Y. Zhang, *Nat Nanotechnol* **2014**, *9*, 372-377; b) H. Liu, Y. Du, Y. Deng and P. D. Ye, *Chem Soc Rev* **2015**, *44*, 2732-2743.
[4] a) Y. Zhang, Y. Zheng, K. Rui, H. H. Hng, K. Hippalgaonkar, J. Xu, W. Sun, J. Zhu, Q. Yan and W. Huang, *Small* **2017**, *13*; b) J. Sun, H. W. Lee, M. Pasta, H. Yuan, G. Zheng, Y. Sun, Y. Li and Y. Cui, *Nat Nanotechnol* **2015**, *10*, 980-985.
[5] F. Xia, H. Wang and Y. Jia, *Nat Commun* **2014**, *5*, 4458.
[6] a) M. van Druenen, F. Davitt, T. Collins, C. Glynn, C. O'Dwyer, J. D. Holmes and G. Collins, *Langmuir* **2019**, *35*, 2172-2178; b) J. Plutnar, Z. Sofer and M. Pumera, *ACS Nano* **2018**, *12*, 8390-8396; c) J. O. Island, G. A. Steele, H. S. J. v. d. Zant and A. Castellanos-Gomez, *2D Materials* **2015**, *2*, 011002.
[7] a) C. R. Ryder, J. D. Wood, S. A. Wells, Y. Yang, D. Jariwala, T. J. Marks, G. C. Schatz and M. C. Hersam, *Nat Chem* **2016**, *8*, 597-602; b) Z. Sofer, J. Luxa, D. Bousa, D. Sedmidubsky, P. Lazar, T. Hartman, H. Hardtdegen and M. Pumera, *Angew Chem Int Ed Engl* **2017**, *56*, 9891-9896; c) M. van Druenen, F. Davitt, T. Collins, C. Glynn, C. O'Dwyer, J. D. Holmes and G. Collins, *Chemistry of Materials* **2018**, *30*, 4667-4674; d) S. Wild, M. Fickert, A. Mitrovic, V. Lloret, C. Neiss, J. A. Vidal-Moya, M. A. Rivero-Crespo, A. Leyva-Perez, K. Werbach, H. Peterlik, M. Grabau, H. Wittkamper, C. Papp, H. P. Steinruck, T. Pichler, A. Gorling, F. Hauke, G. Abellan and A. Hirsch, *Angew Chem Int Ed Engl* **2019**, *58*, 5763-5768; e) S. Thurakkal and X. Zhang, *Adv Sci (Weinh)* **2020**, *7*, 1902359; f) C. Huang, S. Hu, X. Zhang, H. Cui, L. Wu, N. Yang, W. Zhou, P. K. Chu and X. F. Yu, *Biosens Bioelectron* **2020**, *165*, 112384; g) R. Guo, Y. Zheng, Z. Hu, J. Zhang, C. Han, E. Longhi, S. Barlow, S. R. Marder and W. Chen, *Chemistry* **2020**, *26*, 6576-6582; h) S. Wild, X. T. Dinh, H. Maid, F. Hauke, G. Abellan and A. Hirsch, *Angew Chem Int Ed Engl* **2020**; i) B. Han, Z. Duan, J. Xu, Y. Zhu, Q. Xu, H. Wang, H. Tai, J. Weng and Y. Zhao, *Advanced Functional Materials* **2020**, *30*, 2002232; j) C. Jellett, J. Plutnar and M. Pumera, *ACS Nano* **2020**, *14*, 7722-7733; k) A. E. Del Río Castillo, C. D. Reyes-Vazquez, L. E. Rojas-Martinez, S. B. Thorat, M. Serri, A. L. Martinez-Hernandez, C. Velasco-Santos, V. Pellegrini and F. Bonaccorso, *FlatChem* **2019**, *18*, 100131.
[8] a) G. Abellan, P. Ares, S. Wild, E. Nuin, C. Neiss, D. R. Miguel, P. Segovia, C. Gibaja, E. G. Michel, A. Gorling, F. Hauke, J. Gomez-Herrero, A. Hirsch and F. Zamora, *Angew Chem Int Ed Engl* **2017**, *56*, 14389-14394; b) R. Gusmao, Z. Sofer and M. Pumera, *ACS Nano* **2018**, *12*, 5666-5673.
[9] a) D. Hanlon, C. Backes, E. Doherty, C. S. Cucinotta, N. C. Berner, C. Boland, K. Lee, A. Harvey, P. Lynch, Z. Gholamvand, S. Zhang, K. Wang, G. Moynihan, A. Pokle, Q. M. Ramasse, N. McEvoy, W. J. Blau, J. Wang, G. Abellan, F. Hauke, A. Hirsch, S. Sanvito, D. D. O'Regan, G. S. Duesberg, V. Nicolosi and J. N. Coleman, *Nat Commun* **2015**, *6*, 8563; b) G. Abellan, S. Wild, V. Lloret, N. Scheuschner, R. Gillen, U. Mundloch, J. Maultzsch, M. Varela, F. Hauke and A. Hirsch, *J Am Chem Soc* **2017**, *139*, 10432-10440.
[10] a) E. Passaglia, F. Cicogna, F. Costantino, S. Coiai, S. Legnaioli, G. Lorenzetti, S. Borsacchi, M. Geppi, F. Telesio, S. Heun, A. Ienco, M. Serrano-Ruiz and M. Peruzzini, *Chem Mater* **2018**, *30*, 2036-2048; b) Y. Cao, X. Tian, J. Gu, B. Liu, B. Zhang, S. Song, F. Fan and Y. Chen, *Angew Chem Int Ed Engl* **2018**, *57*, 4543-4548; c) Y. Zhang, N. Dong, H. Tao, C. Yan, J. Huang, T. Liu, A. W. Robertson, J. Texter, J. Wang and Z. Sun, *Chemistry of Materials* **2017**, *29*, 6445-6456; d) D. An, J. Fu, Z. Xie, C. Xing, B. Zhang, B. Wang and M. Qiu, *J Mater Chem B* **2020**, *8*, 7076-7120.
[11] a) X. Tang, W. Liang, J. Zhao, Z. Li, M. Qiu, T. Fan, C. S. Luo, Y. Zhou, Y. Li, Z. Guo, D. Fan and H. Zhang, *Small* **2017**, *13*; b) J. Plutnar, J. Šturala, V. Mazánek, Z. Sofer and M. Pumera, *Advanced Functional Materials* **2018**, *28*, 1801438; c) Y. L. Hsieh, W. H. Su, C. C. Huang and C. Y. Su, *ACS Appl Mater Interfaces* **2020**, *12*, 37375-37383.
[12] P. G. Yajuan Liu, Taiming Zhang, Xianjun Zhu, Mengmeng Zhang, Muqing Chen, Pingwu and G.-W. W. Du, Hengxing Ji, Jinlong Yang, and Shangfeng Yang, *Angewandte Chemie International Edition* **2019**, *58*, 1479-1483.
[13] a) L. M. Viculis, J. J. Mack, O. M. Mayer, H. T. Hahn and R. B. Kaner, *Journal of Materials Chemistry* **2005**, *15*, 974; b) E. Yoo, Kim, J., Hosono, E., Zhou, H.S., Kudo, T. and Honma, I., *Nano Lett* **2008**, *8*, 2277-2282; c) J. M. Englert, C. Dotzer, G. Yang, M. Schmid, C. Papp, J. M. Gottfried, H. P. Steinruck, E. Spiecker, F. Hauke and A. Hirsch, *Nat Chem* **2011**, *3*, 279-286.
[14] a) G. Abellan, C. Neiss, V. Lloret, S. Wild, J. C. Chacon-Torres, K. Werbach, F. Fedi, H. Shiozawa, A. Gorling, H. Peterlik, T. Pichler, F. Hauke and A. Hirsch, *Angew Chem Int Ed Engl* **2017**, *56*, 15267-15273; b) A. Ng, T. E. Sutto, B. R. Matis, Y. Deng, P. D. Ye, R. M. Stroud, T. H. Brintlinger and N. D. Bassim, *Nanotechnology* **2017**, *28*, 155601.
[15] a) X. Ren, P. Lian, D. Xie, Y. Yang, Y. Mei, X. Huang, Z. Wang and X. Yin, *Journal of Materials Science* **2017**, *52*, 10364-10386; b) R. Zhang, J. Waters, A. K. Geim and I. V. Grigorieva, *Nat Commun* **2017**, *8*, 15036.
[16] C. Wang, Q. He, U. Halim, Y. Liu, E. Zhu, Z. Lin, H. Xiao, X. Duan, Z. Feng, R. Cheng, N. O. Weiss, G. Ye, Y. C. Huang, H. Wu, H. C. Cheng, I. Shakir, L. Liao, X. Chen, W. A. Goddard, III, Y. Huang and X. Duan, *Nature* **2018**, *555*, 231-236.
[17] R. Jain, Y. Singh, S.-Y. Cho, S. P. Sasikala, S. H. Koo, R. Narayan, H.-T. Jung, Y. Jung and S. O. Kim, *Chemistry of Materials* **2019**, *31*, 2786-2794.
[18] a) Z. Huang, H. Hou, Y. Zhang, C. Wang, X. Qiu and X. Ji, *Adv Mater* **2017**, *29*; b) J. Li, C. Chen, S. Liu, J. Lu, W. P. Goh,

H. Fang, Z. Qiu, B. Tian, Z. Chen, C. Yao, W. Liu, H. Yan, Y. Yu, D. Wang, Y. Wang, M. Lin, C. Su and J. Lu, *Chemistry of Materials* **2018**, *30*, 2742-2749.
[19] a) A. J. Cooper, M. Velický, I. A. Kinloch and R. A. W. Dryfe, *Journal of Electroanalytical Chemistry* **2014**, *730*, 34-40; b) Z. Chen, D. Guo, L. Si and G. Xie, *Scanning* **2017**, *2017*, 9438573; c) L. Wei, F. Wu, D. Shi, C. Hu, X. Li, W. Yuan, J. Wang, J. Zhao, H. Geng, H. Wei, Y. Wang, N. Hu and Y. Zhang, *Sci Rep* **2013**, *3*, 2636; d) W. Sirisaksoontorn, A. A. Adenuga, V. T. Remcho and M. M. Lerner, *J Am Chem Soc* **2011**, *133*, 12436-12438; e) Y. L. Zhong and T. M. Swager, *J Am Chem Soc* **2012**, *134*, 17896-17899.
[20] a) H. Xu and K. S. Suslick, *J Am Chem Soc* **2011**, *133*, 9148-9151; b) A. M. Gravagnuolo, E. Morales-Narváez, S. Longobardi, E. T. da Silva, P. Giardina and A. Merkoçi, *Advanced Functional Materials* **2015**, *25*, 2771-2779.
[21] W. Huang, Lin, Y., Taylor, S., Gaillard, J., Rao, A. M., & Sun, Y.-P. , *Nano Lett* **2002**, *2*, 31-234.
[22] K. L. Kuntz, R. A. Wells, J. Hu, T. Yang, B. Dong, H. Guo, A. H. Woomer, D. L. Druffel, A. Alabanza, D. Tomanek and S. C. Warren, *ACS Appl Mater Interfaces* **2017**, *9*, 9126-9135.
[23] L. Koefoed, S. U. Pedersen and K. Daasbjerg, *Langmuir* **2017**, *33*, 3217-3222.
[24] J. Chattopadhyay, Sadana, A. K., Liang, F., Beach, J. M., Xiao, Y., Hauge, R. H., & Billups, W. E. , *Organic Letters* **2005**, *7*, 4067-4069.
[25] G. Abellan, M. Schirowski, K. F. Edelthalhammer, M. Fickert, K. Werbach, H. Peterlik, F. Hauke and A. Hirsch, *J Am Chem Soc* **2017**, *139*, 5175-5182.
[26] L. Wang, Z. Sofer and M. Pumera, *ChemElectroChem* **2015**, *2*, 324-327.
[27] A. Favron, E. Gaufres, F. Fossard, A. L. Phaneuf-L'Heureux, N. Y. Tang, P. L. Levesque, A. Loiseau, R. Leonelli, S. Francoeur and R. Martel, *Nat Mater* **2015**, *14*, 826-832.
[28] A. J. Cooper, N. R. Wilson, I. A. Kinloch and R. A. W. Dryfe, *Carbon* **2014**, *66*, 340-350.
[29] a) M. N. Ahmed, K. A. Yasin, S. Hameed, K. Ayub, I.-u. Haq, M. N. Tahir and T. Mahmood, *Journal of Molecular Structure* **2017**, *1129*, 50-59; b) R. Kumar, S. Sharma, D. Pathak, N. Dhiman and N. Arora, *Solid State Ionics* **2017**, *305*, 57-62.
[30] a) K. E. O'Harra, I. Kammakakam, J. E. Bara and E. M. Jackson, *Polymer International* **2019**, *68*, 1547-1556; b) N. M. Logacheva, V. E. Baulin, A. Y. Tsivadze, E. N. Pyatova, I. S. Ivanova, Y. A. Velikodny and V. V. Chernyshev, *Dalton Trans* **2009**, 2482-2489.
[31] N. Colthup, *Introduction to Infrared and Raman Spectroscopy*, Elsevier, **2012**, p.
[32] K. Zhang, *Chemically Derived Graphene: Functionalization, Properties and Applications*, RSC Publishing, **2018**, p.
[33] R. Ma and T. Sasaki, *Acc Chem Res* **2015**, *48*, 136-143.
[34] Y. S. Ebina, T., Watanabe, M., *Solid State Ionics* **2002**, *151*, 177-182.
[35] H. Zhu, P. Huang, L. Jing, T. Zuo, Y. Zhao and X. Gao, *J. Mater. Chem.* **2012**, *22*, 2063-2068.
[36] F. M. Koehler, A. Jacobsen, T. Ihn, K. Ensslin and W. J. Stark, *Nanoscale* **2012**, *4*, 3781-3785.
[37] a) E. Bjerglund, M. Kongsfelt, K. Shimizu, B. B. Jensen, L. Koefoed, M. Ceccato, T. Skrydstrup, S. U. Pedersen and K. Daasbjerg, *Langmuir* **2014**, *30*, 6622-6628; b) R. Sharma, J. H. Baik, C. J. Perera and M. S. Strano, *Nano Lett* **2010**, *10*, 398-405; c) J. R. Lomeda, Doyle, C. D., Kosynkin, D. V., Hwang, W.-F., & Tour, J. M. , *J Am Chem Soc* **2008**, *130*, 16201-16206.
[38] V. Artel, Q. Guo, H. Cohen, R. Gasper, A. Ramasubramaniam, F. Xia and D. Naveh, *npj 2D Materials and Applications* **2017**, *1*.
[39] A. E. Del Rio Castillo, V. Pellegrini, H. Sun, J. Buha, D. A. Dinh, E. Lago, A. Ansaldo, A. Capasso, L. Manna and F. Bonaccorso, *Chem. Mater.* **2018**.
[40] S. Wu, F. He, G. Xie, Z. Bian, J. Luo and S. Wen, *Nano Lett* **2018**, *18*, 5618-5627.
[41] M. T. Edmonds, A. Tadich, A. Carvalho, A. Ziletti, K. M. O'Donnell, S. P. Koenig, D. F. Coker, B. Ozyilmaz, A. H. Neto and M. S. Fuhrer, *ACS Appl Mater Interfaces* **2015**, *7*, 14557-14562.